MSFEM and MOR to Minimize the Computational Costs of Nonlinear Eddy-Current Problems in Laminated Iron Cores

K. Hollaus, J. Schöberl, and M. Schöbinger

Institute for Analysis and Scientific Computing, Technische Universität Vienna, A-1040 Vienna, Austria

The multiscale finite-element method (MSFEM) reduces the computational costs for the simulation of eddy currents (ECs) in laminated iron cores compared with the standard finite-element method (SFEM) essentially. Nevertheless, the complexity of the resulting problem is still too large to solve it conveniently. The idea is to additionally exploit model order reduction (MOR). Snapshots (SNSs) for a reduced basis are cheaply calculated by the MSFEM. Numerical simulations of a small transformer show exceptional performance. This is well demonstrated by the overall EC losses and by the distribution of the magnetic-flux density, both with respect to those obtained by the MSFEM.

***Index Terms*— Laminated iron core, model order reduction (MOR), multiscale finite-element method (MSFEM), nonlinear eddy-current problem (ECP), time-stepping method.**

I. Introduction

AN ACCURATE and efficient simulation of the eddy currents (ECs) in laminated iron cores by the finite-element method (FEM) is of great interest in the design of electrical devices. However, the dimensions of such cores are extremely different. The overall dimensions are in the range of meters, whereas the thickness of the laminates and the width of the gaps between them are in the sub-millimeter range. Moreover, the magnetic properties of iron are highly nonlinear. Modeling of each laminate of an iron core by finite elements would lead to extremely large nonlinear systems of equations impossible to reasonably solve with present computer resources.

The multiscale FEM (MSFEM) makes use of the quasi-periodic structure of laminated cores and reduces the computational costs essentially without loosing accuracy [1], [2] compared with the standard FEM (SFEM). Although the MSFEM has brought a great progress in solving the EC problem (ECP) in laminated cores, the complexity of the MSFEM models is still too large to become a routine task for engineers.

The model order reduction (MOR) has proven to be a powerful tool to drastically reduce the costs in solving linear problems in computational electromagnetics. Proper orthogonal decomposition (POD) based the MOR on using snapshots (SNSs) to select an optimal basis for the reduced model. This has been applied to solve large-scale linear problems very successfully [3].

Strategies to select an optimal number of SNSs except those considering simply the dominant eigenvectors with the largest singular values can be found, for instance, in [3] and [4].

However, nonlinear problems are still extremely challenging [5], [6]. The by far more demanding nonlinear ECPs are currently under intensive investigations, as can be seen in [4], [7], and [8]. The need to assemble the original high-dimensional system matrix results in a moderate speedup. To overcome this limitation, for example, the discrete empirical interpolation method or the dynamic mode decomposition have been employed [5], [9].

A serious problem of the previous methods is that the projection is valid only for the space spanned by the SNSs. These methods fail once the system leaves this space. To overcome this problem, the nonlinear system has been reformulated in such a way that the quadratic-bilinear differential algebraic equations are obtained [4], [7]. To this end, the nonlinear BH-curve is approximated by a polynomial representation.

The MOR for the nonlinear systems arising from the MSFEM of the ECPs in laminated iron has not been addressed so far. The idea of this article is to exploit the MSFEM for laminated cores to compute a few SNSs at selected time instants for the reduced basis of a large nonlinear problem with reasonable effort. Then, time stepping with small time steps is carried out using this reduced basis. The MOR has also been applied to facilitate the simulations of electrical machines [9]–[11].

The error associated with the MSFEM and the MOR has been investigated by the overall EC losses and by the distribution of the magnetic-flux density by means of the single-phase transformer shown in Fig. 1. The numerical results are excellent.

II. Eddy-Current Problem

The nonlinear ECP in the time domain

$$\begin{aligned} \operatorname{curl} \mu^{-1}(\mathbf{A}) \operatorname{curl} \mathbf{A} + \sigma \frac{\partial}{\partial t}\mathbf{A} &= \boldsymbol{J}_0 \quad \text{in } \Omega = \Omega_c \cup \Omega_0 \\ \boldsymbol{A} \times \boldsymbol{n} &= \mathbf{0} \quad \text{on } \Gamma_D \\ \mu^{-1}(\mathbf{A}) \operatorname{curl} \boldsymbol{A} \times \boldsymbol{n} &= \mathbf{0} \quad \text{on } \Gamma_N \end{aligned} \tag{1}$$

where $\boldsymbol{A}$ is the magnetic vector potential, $\boldsymbol{J}_0$ stands for the known currents in coils, Ω_c represents the conducting domain (iron), and Ω_0 the non-conducting domain (air), has to be solved. The boundary conditions in (1) represent three

Manuscript received August 19, 2019; revised November 6, 2019; accepted November 9, 2019. Date of current version January 20, 2020. Corresponding author: K. Hollaus (e-mail: karl.hollaus@tuwien.ac.at).

Color versions of one or more of the figures in this article are available online at http://ieeexplore.ieee.org.

Digital Object Identifier 10.1109/TMAG.2019.2954392

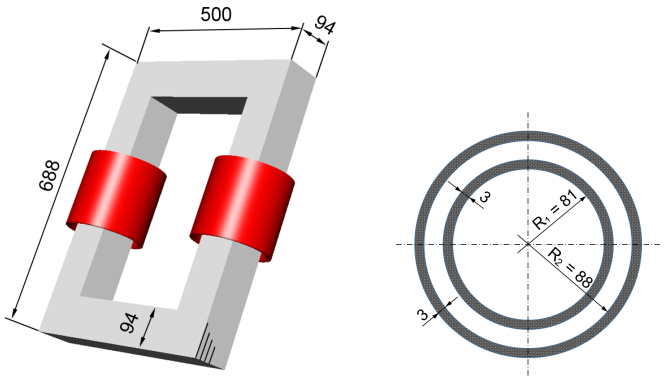

Fig. 1. Single-phase transformer (left) and cross section of the cylindrical coil (right, not to scale); dimensions in mm.

planes of symmetry for the numerical example in Section V, and Γ_D includes also the far boundary.

The weak form reads as follows.

Find $\boldsymbol{A}_h \in V_0 := \{\boldsymbol{A}_h \in \mathcal{V}_h : \boldsymbol{A}_h \times \boldsymbol{n} = \boldsymbol{0} \text{ on } \Gamma_D\}$, such that

$$\int_\Omega \mu^{-1}(\boldsymbol{A}_h)\,\mathrm{curl}\,\boldsymbol{A}_h \cdot \mathrm{curl}\,\boldsymbol{v}_h\,d\Omega + \int_{\Omega_c} \sigma \frac{\partial}{\partial t}\boldsymbol{A}_h \cdot \boldsymbol{v}_h\,d\Omega + \int_{\Omega_0} \sigma_0 \frac{\partial}{\partial t}\boldsymbol{A}_h \cdot \boldsymbol{v}_h\,d\Omega = \int_\Omega \boldsymbol{J}_0 \cdot \boldsymbol{v}_h\,d\Omega \quad (2)$$

for all $\boldsymbol{v}_h \in V_0$, where $\mathcal{V}_h \subset H(\mathrm{curl}, \Omega)$.

Regularization with $0 < \sigma_0 \ll \sigma$ has been applied in air to obtain a unique solution. Solutions of (2) with the SFEM have been used to substantiate the accuracy of the solutions obtained by the MSFEM [12].

III. Multiscale FEM

The solution of (2) characterized by the large scale of the laminated iron core and the small scale with the quasi-periodic structure of the lamination leads to the first-order multiscale approach

$$\tilde{\boldsymbol{A}} = \boldsymbol{A}_0 + \phi_1 \boldsymbol{A}_1 + \mathrm{grad}\,(\phi_1 w_1) \quad (3)$$

representing the trial function and the test function

$$\tilde{\boldsymbol{v}} = \boldsymbol{v}_0 + \phi_1 \boldsymbol{v}_1 + \mathrm{grad}\,(\phi_1 q_1) \quad (4)$$

with the same structure. The multiscale approach is marked by the tilde.

The laminated domain Ω_m consists of iron laminates and air gaps in between. $\boldsymbol{A}_1$, w_1, and ϕ_1 are restricted to Ω_m, whereas $\boldsymbol{A}_0$ is valid in the entire domain $\Omega = \Omega_m \cup \Omega_0$. Essential boundary conditions are prescribed by means of $\boldsymbol{A}_0$ exclusively, and only natural boundary conditions are provided for $\boldsymbol{A}_1$ and w_1.

A detailed explanation of the corresponding weak form, of the micro-shape function ϕ_1 and the meaning of the components $\boldsymbol{A}_0$, $\boldsymbol{A}_1$, and w_1 can be found in [12].

The weak form reads as follows.

Find $(\boldsymbol{A}_{0h}, \boldsymbol{A}_{1h}, w_{1h}) \in V_0 := \{(\boldsymbol{A}_{0h}, \boldsymbol{A}_{1h}, w_{1h}) : \boldsymbol{A}_{0h} \in \mathcal{U}_h, \boldsymbol{A}_{1h} \in \mathcal{V}_h, w_{1h} \in \mathcal{W}_h \text{ and } \boldsymbol{A}_{0h} \times \boldsymbol{n} = \boldsymbol{0} \text{ on } \Gamma_D\}$, such that

$$\int_\Omega \mu^{-1}(\tilde{\boldsymbol{A}}_h)\,\mathrm{curl}(\tilde{\boldsymbol{A}}_h) \cdot \mathrm{curl}(\tilde{\boldsymbol{v}}_h)\,d\Omega + \int_{\Omega_c} \sigma \frac{\partial}{\partial t}\tilde{\boldsymbol{A}}_h \cdot \tilde{\boldsymbol{v}}_h\,d\Omega + \int_{\Omega_0} \sigma_0 \frac{\partial}{\partial t}\boldsymbol{A}_{0h} \cdot \boldsymbol{v}_{0h}\,d\Omega = \int_\Omega \boldsymbol{J}_0 \cdot \tilde{\boldsymbol{v}}_{0h}\,d\Omega \quad (5)$$

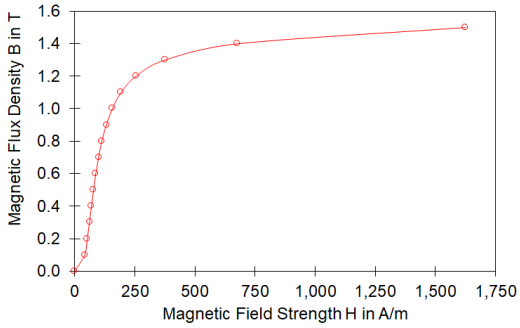

Fig. 2. Magnetization curve, convex–concave.

for all $(\boldsymbol{v}_{0h}, \boldsymbol{v}_{1h}, q_{1h}) \in V_0$, where $\mathcal{U}_h \subset H(\mathrm{curl}, \Omega)$, $\mathcal{V}_h \subset H(\mathrm{curl}, \Omega_m)$, and $\mathcal{W}_h \subset H^1(\Omega_m)$ have been selected.

The micro-shape function ϕ_1 is a periodic, piecewise linear, and continuous function, i.e., $\phi_1 \in H_{\mathrm{per}}(\Omega_m)$. The arising coefficients in (5) have been averaged see [12].

IV. Model Order Reduction

The MSFEM (5) results in the nonlinear equation system

$$A(\mu)x = f. \quad (6)$$

The dimension of the matrix A is $n \times n$ degrees of freedom (DOFs), and the permeability μ in (6) indicates the nonlinearity.

An SNS matrix

$$S = (x_1, x_2, \ldots, x_m) \quad (7)$$

is assembled by m SNSs x_i as column vectors. The SNSs are the solutions of $A_i(\mu)x_i = f_i$ for input currents feeding the coils at m time instants (see Section VI-A). The dimension of S is equal to $n \times m$, where $n \gg m$ holds. No POD has been carried out in this article. Thus, (7) has been used as projection matrix W, i.e., $W = S$.

Using $x = Wy$, the large system (6) becomes the reduced model

$$Ky = g \quad (8)$$

with $K = W^T A W$ and $g = W^T f$.

V. Numerical Example

Although the transformer in Fig. 1 is described in detail in [12], for the sake of convenience, it is presented here again. The core is composed of 183 laminates with a fill factor of $k_f = 0.9734$. The cross section of a cylinder-shaped coil is shown in Fig. 1. It consists of two layers (dark rings), 60 turns per layer. The length of the coil is equal to 192 mm. The arrangement of the core with the coils exhibits three planes of symmetry. One-eighth of the problem has been considered in the simulations. The iron is highly nonlinear, but assumed to be isotropic. The magnetization curve considered in the simulations is determined by measurement points (see Fig. 2). The curve is convex–concave. A conductivity of $\sigma = 2.0 \times 10^6$ S/m has been selected.

To avoid the modeling of the coils, the Biot–Savart field was exploited. The values of the input current I are selected with

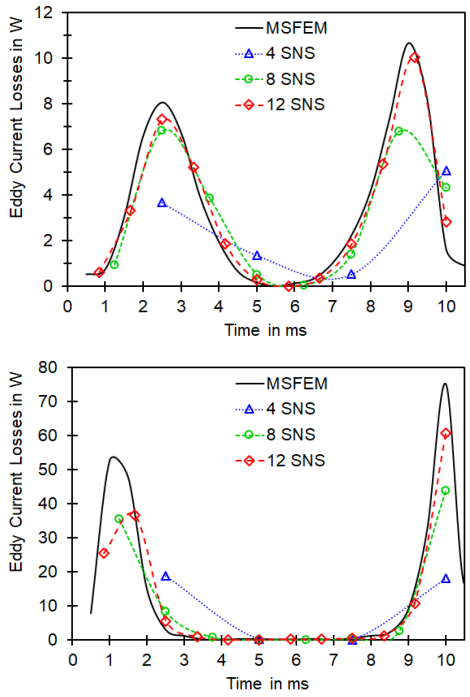

Fig. 3. EC losses for different input currents $I = 1$ A (above) and $I = 3$ A (below) and the respective SNSs [4 (blue), 8 (green), and 12 (red)] selected at equidistant time instants within the first half-period.

TABLE I
NUMBER OF UNKNOWN DOFS

Method(s)	SFEM	MSFEM	MSFEM and MOR
DOFs	1,116,860	103,879	4, 8 or 12

1.0, 2.0, and 3.0 A (peak value) to deal with different states of saturation. Simulations with these currents have been carried out for 50 Hz. The implicit Euler scheme has been used for the time-stepping method and the fixed-point method [13] to solve the nonlinear system resulting from the MSFEM.

VI. NUMERICAL RESULTS

Due to the lack of space, sometimes, only low ($I = 1$ A) and high ($I = 3$ A) saturations are presented.

A. Selection of the SNSs

SNSs have been computed with the time steps of 2.5, 1.25, and 0.8333 ms, respectively, for 4, 8, and 12 SNSs, respectively, within the first half-period in time with the MSFEM in a pre-processing phase instead of simply taking the first computed solutions in the actual time-stepping procedure (see Fig. 3). The transient behavior of the losses and the influence of the non-linearity are clearly visible for different input currents I. The MSFEM is essentially cheaper to compute SNSs than the SFEM, compared with Table I. The influence of the selection of the time instants is shown in Fig. 4 by means of 12 SNSs.

B. Error in the Overall Losses P

Although some of the individual losses corresponding to SNSs in VI-A clearly deviate from the reference losses obtained by the MSFEM, as can been seen in Fig. 3, the losses obtained by the MOR with these SNSs hardly show a deviation

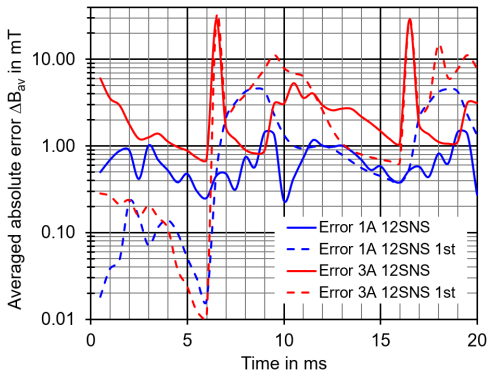

Fig. 4. Influence of the selection of 12 SNSs for different input currents [$I = 1$ A (blue) and $I = 3$ A (red)] first means that the solutions of the first 12 time instants are chosen as SNSs; otherwise, the 12 SNSs are chosen at equidistant time instants within the first half-period.

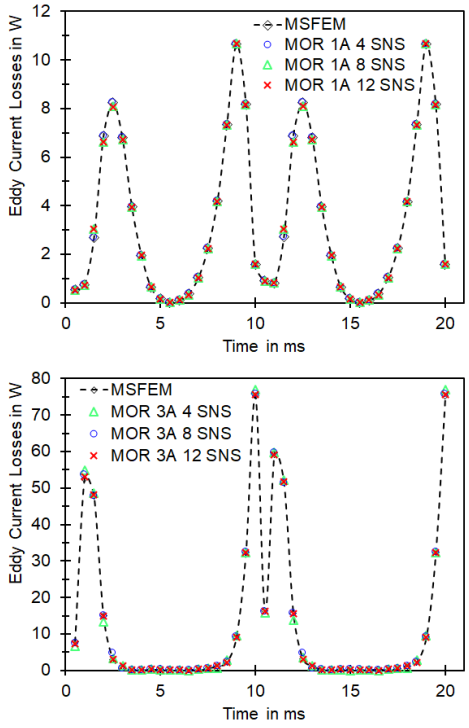

Fig. 5. EC losses for $I = 1$ A (above) and $I = 3$ A (below) obtained by different number of SNSs.

and agree well with the reference losses calculated with the MSFEM shown in Fig. 5. The relative error with four SNSs is in general small, but large for small losses and sometimes almost at 30% (see Fig. 6). Using 8 or 12 SNSs provides an exceptionally small overall relative error. The relative error is almost always well below 1%. This holds for low saturation, i.e., $I = 1$ A. In the case of higher saturation, the relative error in the losses becomes sometimes large, where the overall losses are very small.

C. Error in the Distribution of the Magnetic-Flux Density B

To additionally study the accuracy of the proposed method, the averaged absolute error

$$\Delta B_{\mathrm{av}} = \sqrt{\frac{1}{\Omega_m} \int_{\Omega_m} (\boldsymbol{B}_{\mathrm{MS}} - \boldsymbol{B}_{\mathrm{MOR}}) \cdot (\boldsymbol{B}_{\mathrm{MS}} - \boldsymbol{B}_{\mathrm{MOR}})\, d\Omega} \tag{9}$$

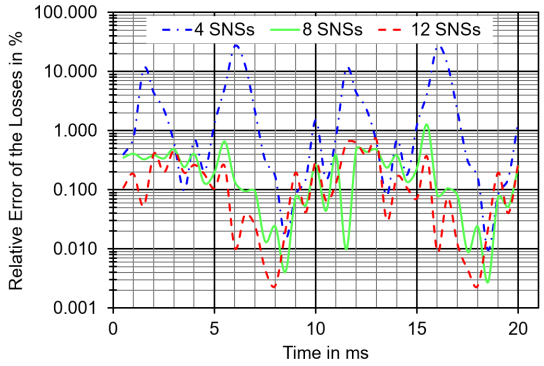

Fig. 6. Relative error in EC losses with $I = 1$ A obtained by different numbers of SNSs.

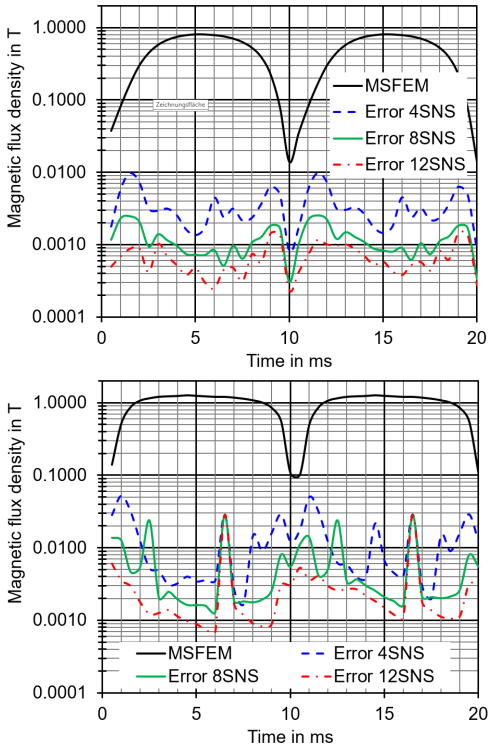

Fig. 7. Average magnetic-flux density $\boldsymbol{B}_{\text{av}}$ (black) for different input currents [$I = 1$ A (above) and $I = 3$ A (below)] and the respective differences ΔB_{av} for different number of SNSs [4 (blue), 8 (green), and 12 (red)].

and, for the sake of comparison, the averaged magnetic-flux density

$$B_{\text{av}} = \sqrt{\frac{1}{\Omega_m} \int_{\Omega_m} \boldsymbol{B}_{\text{MS}} \cdot \boldsymbol{B}_{\text{MS}} \, d\Omega} \tag{10}$$

have been calculated and presented in Fig. 7. Integration has been carried out on the finite-element mesh used for the reference solutions based on the SFEM [12]. Absolute errors are shown in Fig. 8. The selected time instants coincide with the first peak value of the respective ΔB_{av} for $I = 3$ A in Fig. 7.

VII. Computational Costs

The required number of DOFs is summarized in Table I. It shows clearly the reduction in the size of the system of

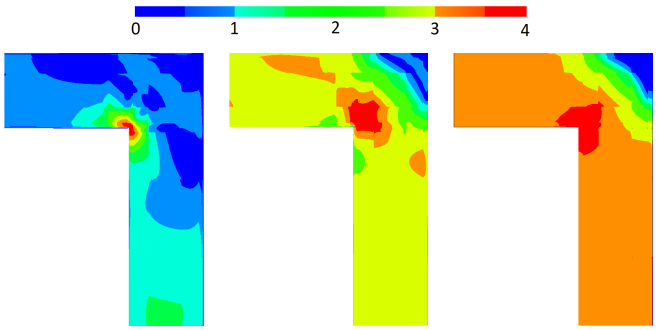

Fig. 8. Absolute error $|\boldsymbol{B}_{\text{MS}} - \boldsymbol{B}_{\text{MOR}}|$ for $I = 3$ A in the outermost laminate (scale above is used as reference): four SNSs at 1.0 ms (0.0–0.4 T, left), eight SNSs at 2.5 ms (0.0–0.04 T, middle), and 12 SNSs at 6.5 ms (0.0–0.04 T, right).

equations to be solved. The total number of nonlinear iterations is 158 for the MSFEM only and 175 for the MSFEM with the MOR with eight SNSs for 40 time steps and $I = 1$ A for the first period. Similar results have been observed for simulations with $I = 2$ A and $I = 3$ A.

Acknowledgment

This work was supported by the Austrian Science Fund (FWF) under Project P 31926.

References

[1] P. Dular, "A time-domain homogenization technique for lamination stacks in dual finite element formulations," *J. Comput. Appl. Math.*, vol. 215, no. 2, pp. 390–399, Jun. 2008.

[2] K. Hollaus and J. Schöberl, "Some 2-D multiscale finite-element formulations for the eddy current problem in iron laminates," *IEEE Trans. Magn.*, vol. 54, no. 4, Apr. 2018, Art. no. 7401716.

[3] Y. Sato and H. Igarashi, "Model reduction of three-dimensional eddy current problems based on the method of snapshots," *IEEE Trans. Magn.*, vol. 49, no. 5, pp. 1697–1700, May 2013.

[4] D. Klis, S. Burgard, O. Farle, and R. Dyczij-Edlinger, "A self-adaptive model-order reduction algorithm for nonlinear eddy-current problems based on quadratic–bilinear modeling," *IEEE Trans. Magn.*, vol. 52, no. 3, Mar. 2016, Art. no. 7201004.

[5] T. Henneron and S. Clénet, "Model order reduction of non-linear magnetostatic problems based on POD and DEI methods," *IEEE Trans. Magn.*, vol. 50, no. 2, Feb. 2014, Art. no. 7000604.

[6] A. Pierquin, T. Henneron, and S. Clénet, "Data-driven model-order reduction for magnetostatic problem coupled with circuit equations," *IEEE Trans. Magn.*, vol. 54, no. 3, Mar. 2018, Art. no. 7201404.

[7] L. Codecasa, "Novel approach to model order reduction for nonlinear eddy-current problems," *IEEE Trans. Magn.*, vol. 51, no. 3, Mar. 2015, Art. no. 7202204.

[8] Y. Sato, M. Clemens, and H. Igarashi, "Adaptive subdomain model order reduction with discrete empirical interpolation method for nonlinear magneto-quasi-static problems," *IEEE Trans. Magn.*, vol. 52, no. 3, Mar. 2016, Art. no. 1100204.

[9] S. Paul and J. Chang, "Fast numerical analysis of electric motor using nonlinear model order reduction," *IEEE Trans. Magn.*, vol. 54, no. 3, Mar. 2018, Art. no. 8101404.

[10] M. Farzamfar, A. Belahcen, P. Rasilo, S. Clénet, and A. Pierquin, "Model order reduction of electrical machines with multiple inputs," *IEEE Trans. Ind. Appl.*, vol. 53, no. 4, pp. 3355–3360, Jul./Aug. 2017.

[11] Z. Bontinck, O. Lass, S. Schöps, and O. Rain, "Model order reduction for rotating electrical machines," May 2017, *arXiv:1705.03872*. [Online]. Available: https://arxiv.org/abs/1705.03872

[12] K. Hollaus, "A MSFEM to simulate the eddy current problem in laminated iron cores in 3D," *Int. J. Comput. Math. Elect. Electron. Eng.*, vol. 38, no. 5, pp. 1667–1682, Sep. 2019.

[13] O. Bíró, K. Preis, and K. Preis, "Finite element calculation of time-periodic 3D eddy currents in nonlinear media," in *Advanced Computational Electromagnetics*, T. Homna, Ed. Budapest, Hungary: Elsevier, Jul. 1995, pp. 62–74.